

Computation of extreme heat waves in climate models using a large deviation algorithm

Francesco Ragone^{a,b}, Jeroen Wouters^{a,c,d}, and Freddy Bouchet^a

^aLaboratoire de Physique, Ens de Lyon, Univ Claude Bernard, Univ Lyon, CNRS, F-69342 Lyon, France; ^bDepartment of Earth and Environmental Sciences, University of Milano–Bicocca, Milan, Italy; ^cSchool of Mathematics and Statistics, University of Sydney, Sydney, Australia; ^dMeteorological Institute, University of Hamburg, Hamburg, Germany

This manuscript was compiled on December 27, 2017

Studying extreme events and how they evolve in a changing climate is one of the most important current scientific challenges. Starting from complex climate models, a key difficulty is to be able to run long enough simulations in order to observe those extremely rare events. In physics, chemistry, and biology, rare event algorithms have recently been developed to compute probabilities of events that cannot be observed in direct numerical simulations. Here we propose such an algorithm, specifically designed for extreme heat or cold waves, based on statistical physics. This approach gives an improvement of more than two orders of magnitude in the sampling efficiency. We describe the dynamics of events that would not be observed otherwise. We show that European extreme heat waves are related to a global teleconnection pattern involving North America and Asia. This tool opens up a wide range of new possible studies to quantitatively assess the impact of climate change.

Climate extreme events | Heat waves | Statistical physics | Rare event algorithms | Large deviation theory

Rare events, for instance extreme droughts, heat waves, rainfalls and storms, can have a severe impact on ecosystems and socioeconomic systems (1–3). The Intergovernmental Panel on Climate Change (IPCC) has concluded that strong evidence exists indicating that hot days and heavy precipitation events have become more frequent since 1950 (4, 5). However, the magnitude of possible future changes are still uncertain for classes of events involving more dynamical aspects, like for instance hurricanes or heat waves (4, 6, 7). Estimates of the average time in between two events of the same class, called return time (or return period), is key for assessing the expected changes in extreme events and their impact. This is crucial on a national level when considering adaptation measures and on the international level when designing policy to implement the Paris Agreement, in particular its Art. 8 (https://en.wikisource.org/wiki/Paris_Agreement). Public or private risk managers need to know amplitudes of events with a return time ranging from a few years, to hundreds of thousands of years when the impact might be extremely large.

The 2003 Western European heat wave led to a death toll of more than 70 000 (8). Similarly, the estimated impact of the 2010 Russian heat wave was a death toll of 55,000, an annual crop failure of $\sim 25\%$, more than 1 million ha of burned areas, and \sim US\$15 billion ($\sim 1\%$ of gross domestic product) of total economic loss (9). During that period, the temperature averages over 31 days at some locations were up to 5.5 standard deviations away from the 1970–1999 climate (9). As no event similar to those heat waves has been observed during the last few centuries, no past observations exist that would allow to quantify their return times. If return times cannot be estimated from observations, we must rely on models.

Several scientific barriers need to be overcome, however, before we can obtain quantitative estimates of rare event return times from a model. One of them is that extreme events are observed so rarely that collecting sufficient data to study quantitatively their dynamics is prohibitively costly. This has led authors of past studies to either use models which are of a lesser quality than the up to date IPCC top class models, or to focus on a single or a few events which does not allow for a quantitative statistical assessment. Making progress for this sampling issue would also allow a better understanding of those rare event dynamics, and strengthen future assessment of which class of models is suited for making quantitative predictions.

Rare event algorithms

In physics, chemistry, and biology rare events may matter: even if they occur on time scales much longer than the typical dynamics time scales, they may have a huge impact. During the last decades, new numerical tools, specifically dedicated to the computation of rare events from the dynamics but requiring a considerably smaller computational effort, have been developed. They have been applied for instance to changes of configurations in magnetic systems in situations of first order transitions (10–12), chemical reactions (13), conformational changes of polymer and biomolecules (14–17) and rare events in turbulent flows (18–22). Since their appearance (23), the analysis of these rare event algorithms also became an active mathematical field (24–28). Several strategies prevail, for in-

Significance Statement

We propose an algorithm to sample rare events in climate models that costs hundred to thousand times less than direct sampling of the model. Applied to the study of extreme heat waves, we estimate the probability of events that can not be studied otherwise because they are too rare, and we get a huge ensemble of realizations of extreme event. Using these results, we describe the teleconnection pattern for the extreme European heat waves. This method should change the paradigm for the study of extreme events in climate models: it will allow to study extremes with higher complexity models, to make inter model comparison easier, and to study the dynamics of extreme events with an unprecedented statistics.

FB. proposed the project, initiated and directed the work; F.R., J.W., and F.B. performed research; F.R. made the core of the numerical work that led to the rare event computation of heat waves and the resulting analysis; and F.R., J.W., and F.B. wrote the paper.

¹To whom correspondence should be addressed. Freddy.Bouchet@ens-lyon.fr

stance genetic algorithms where an ensemble of trajectories is evolved and submitted to selections, minimum action methods, or importance sampling approaches.

Here we apply for the first time a rare event algorithm for sampling extreme events in a climate model. Given the complexity of the models and phenomena, this has long been thought to be impracticable for climate applications. A key success factor for this approach is to first clearly identify a restricted class of phenomena for which rare event algorithm may be practicable. Then one has to choose among the dozens of available algorithms which one may be suited for this class of phenomena. Finally one has to develop the tools that will make one specific algorithm effective for climate observables. Matching these idea coming from the rare event community and climate dynamics requires a genuine interdisciplinary approach, in order to both master the climate dynamics phenomenology and the probability concepts related to rare event algorithms. We study extreme heat waves as a robust phenomena in current climate models, involving the largest scales of the turbulent dynamics, and use an algorithm dedicated to study large deviations of time averaged quantities: the Giardina–Kurchan–Lecomte–Tailleur (GKLT) algorithm (29–31). As this algorithm was dedicated to compute large deviation rate functions in the infinite time limit, we have to pick the main ideas of the algorithm, but to twist its usage to compute finite time observables. Moreover, we have to develop a further adaptation, aimed at computing return times rather than large deviation rate functions or tails of probability distribution functions. With this approach, based on statistical physics concepts, we compute the probability of events that cannot be observed directly in the model, the number of observed rare events for a given amplitude is multiplied by several hundreds, and we can predict the return time for events that would require thousand times more computational resources.

The jet stream dynamics and extreme heat waves

Midlatitude atmospheric dynamics is dominated by the jet streams (one per hemisphere). The jet streams are strong and narrow eastward air currents, located at about 45°N or 45°S , with maximum velocity of the order of $40\text{ m}\cdot\text{s}^{-1}$ close to the tropopause (see Fig. 1(a)). The climatological position of the northern hemisphere jet stream in our model is seen on Fig. 1(b), that represents the time average of the kinetic energy due to the horizontal component of the velocity field at 500 hPa pressure surfaces. The jet stream’s meandering dynamics, due to non-linear Rossby waves, is related to the succession of anticyclonic and cyclonic anomalies which characterize weather at midlatitudes. It is well known that midlatitude heat waves, like the 2003 Western European heat wave or the 2010 Russian heat waves, are due to rare and persistent anticyclonic anomalies (or fluctuations), that arise as either Rossby wave breaking (blockings), or shifts of the jet stream, or more complex dynamical events leading to a stationary pattern of the jet stream.

Studying extreme heat waves then amounts to studying the non-linear and turbulent dynamics of the atmosphere. Two key dynamical variables are the temperature and pressure fields. One could look at pressure maps at some value of the geopotential height (the most convenient vertical coordinate). Equivalently, it is customary to look at the geopotential height

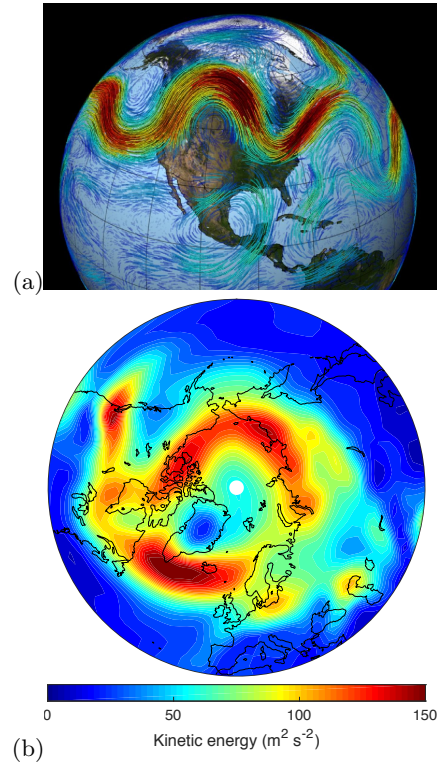


Fig. 1. (a) Snapshot of wind speed velocity at the top of the troposphere, showing the jet stream over North America (from NASA). (b) Average horizontal kinetic energy at 500hPa (mid troposphere) in the Plasim model, showing the averaged Northern Hemisphere jet stream.

value on a surface defined by a fixed pressure.

Heat waves in the Plasim model

We use the Plasim model (Planet Simulator, (32)). Plasim gives a reasonably realistic representation of atmospheric dynamics and of its interactions with the land surface and with the mixed layer of the ocean; it includes parameterizations of radiative transfers and cloud dynamics. While Plasim features about 10^5 degrees of freedoms, it is simpler and less computationally demanding than the top class IPCC models used for assessing the projection of temperature increase. It is nevertheless in the class of models used to discuss extreme heat waves in the last IPCC report (for instance (33)). Our aim is to demonstrate the huge potential of rare event algorithms for this class of models, and to advocate the feasibility of this approach for top class IPCC models in the near future.

Heat waves can be defined as rare and long lasting anomalies (fluctuations) of the surface temperature over an extended area (34, 35). We consider

$$a = \frac{1}{T} \int_0^T \bar{A}(t) dt \quad \text{where} \quad \bar{A}(t) = \frac{1}{\mathcal{A}} \int_{\text{Area}} T_S(\mathbf{r}, t) d\mathbf{r}, \quad [1]$$

where \mathbf{r} is the spatial variable, t is time, and T_S is the surface temperature anomaly with respect to its averaged value, \mathcal{A} is the surface area, and T is the heat wave duration. The relevant value for T depends on the application of interest. We vary T between a few weeks to several months and discuss the results for $T = 90$ days. The spatial average is over Western Europe, the region over land surface with latitudinal and longitudinal

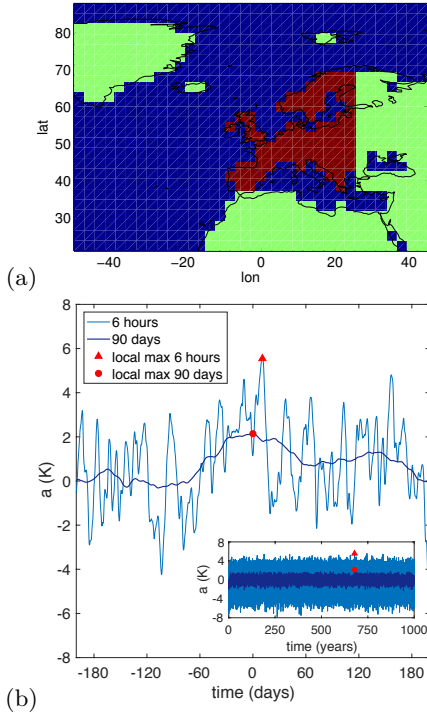


Fig. 2. (a) The red colors marks the Europe area over which the temperature is averaged. (b) Timeseries of European surface temperature anomaly, 6 hours (light blue) and 90 days running mean (dark blue), during 360 days and 1 000 years (inset). The red triangles and circles feature one local maximum of the temperature anomalies, as an example of a 2 K heat wave lasting 90 days.

boundaries 36N-70N and 11W-25E (see Fig. 2(a)). We study the upper tail of the probability distribution function (PDF) of a , denoted $P(a, T)$.

The instantaneous T_S has standard deviation $\sigma \approx 1.6$ K, and is slightly skewed towards positive values. Its autocorrelation time is $\tau_c \approx 7.5$ days, which is the typical time for synoptic fluctuations (at a scale of about 1 000 km). An exam-

ple of a timeseries of the 90 days averaged Europe temperature anomaly is shown on Fig. 2(b).

Importance sampling and large deviations of time averaged temperature

We first explain importance sampling, a crucial probabilistic concept for the following discussion. We sample N independent and identically distributed random numbers from a probability distribution function (PDF) ρ and want to estimate γ_B , the probability to be in a small set B (see Fig. 3(a)). We will obtain about $N\gamma_B$ occurrences in the set B , from which we can estimate γ_B . An easy calculation (24) shows that the relative error of this estimate is of the order of $1/\sqrt{N\gamma_B}$. For instance if γ_B is of the order of 10^{-2} , estimating γ_B with a relative error of 1% requires a huge sample size, of the order of 10^6 . However, if we rather sample N random numbers \tilde{X}_n from the distribution $\tilde{\rho}$ (see Fig. 3(a)), where $\rho(x) = L(x)\tilde{\rho}(x)$, with L conveniently chosen, then the event may become common: this is importance sampling. From the formula $\rho = L\tilde{\rho}$, we have the estimate $\tilde{\gamma}_B = \frac{1}{N} \sum_{n=1}^N L(\tilde{X}_n) 1_B(\tilde{X}_n)$, where 1_B is the indicator function of the set B . If the rare event is actually common for $\tilde{\rho}$, this estimate gives a relative error of order $1/\sqrt{N}$ (see (24) for a precise formula). Then, in order to estimate γ_B with a relative error of 1%, we need a sample size of order of 10^4 ; this is a gain of a factor 100. The importance sampling gain grows like the inverse of the probability γ_B . The key question is: How to perform importance sampling, relevant for extreme heat waves, starting from a climate model?

Since the climate is a non equilibrium dynamical system, importance sampling has to be performed at the level of the trajectories. Trajectories generated by the model are distributed according to the unknown PDF $\mathbb{P}_0(\{X(t)\}_{0 \leq t \leq T} = \{x(t)\}_{0 \leq t \leq T})$ (this is a formal notation for the probability of the model variables $X(t)$ to be close to $x(t)$). We use the GKL large deviation algorithm, described below, that selects trajectories distributed according to the importance sampling PDF \mathbb{P}_k

$$\mathbb{P}_k(\{X(t)\}_{0 \leq t \leq T} = \{x(t)\}_{0 \leq t \leq T}) = \frac{1}{Z(k, T)} \exp\left(k \int_0^T A(X(t)) dt\right) \mathbb{P}_0(\{X(t)\}_{0 \leq t \leq T} = \{x(t)\}_{0 \leq t \leq T}), \quad [2]$$

where k is a real valued parameter, and $Z(k, T)$ is a normalization constant such that \mathbb{P}_k is a normalized PDF. The surface averaged temperature is $\tilde{A}(t) = A(X(t))$. One observes that for positive values of k , the measure \mathbb{P}_k is tilted with respect to \mathbb{P}_0 such that large values of $\int_0^T A(X(t)) dt$ will be favored with an exponential weight. Tuning k , we will study different ranges of extreme values for $a = \frac{1}{T} \int_0^T A(X(t)) dt$, and thus different classes of extreme heat waves when a is the time averaged European temperature (1).

The large deviation algorithm performs an ensemble simulation with N trajectories (ensemble members), typically $N \sim O(10^2 - 10^3)$. The trajectories start from independent initial conditions that sample the model's invariant measure. After time intervals of constant duration τ we stop the simu-

lation, and for each trajectory we compute a score function based on the dynamics in the previous time interval of length τ (see the Supporting Information Appendix for the definition of the score function). Trajectories which are going in the direction of the extremes of interest, as measured by the score function, are cloned in one or more copies, while poorly scoring trajectories are killed. We call this step resampling, and τ the resampling time. The different copies of a successful trajectory are slightly perturbed, so that they can evolve differently. Then the ensemble of trajectories is iterated for another resampling time τ . Once the final time T_a has been reached, resampling is performed one last time. With a proper choice of the score function we obtain an ensemble of N trajectories of length T_a distributed according to equation (2), where k enters as a chosen parameter of the algorithm. The full details of

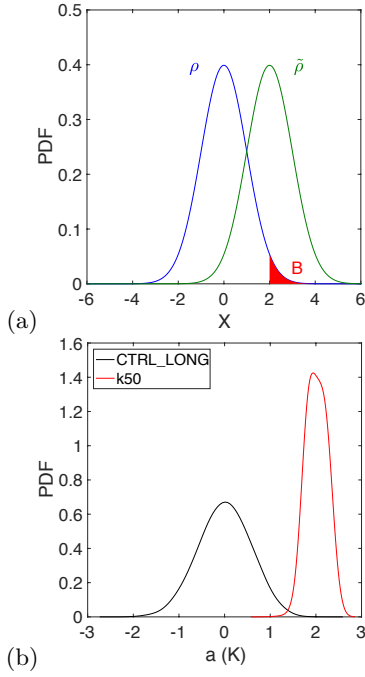


Fig. 3. (a) We want to estimate the probability to be in the set B , for the model PDF $\rho(x)$. We are able to sample instead from the PDF $\tilde{\rho}(x)$ for which the rare event becomes common. We know the relation $L = \rho/\tilde{\rho}$ and can recover the model statistics ρ , from the importance sampling $\tilde{\rho}$. (b) PDF of the time average temperature a ($T = 90$ d) for the model control run (black) and for the algorithm statistics with $k = 50$, illustrating that the algorithm performs importance sampling and that $+2^\circ\text{K}$ heat waves become common for the algorithm while they are rare for the model.

the algorithm implementation are provided in the Supporting Information Appendix.

In the normalization term of (2), $Z(k, T) = \mathbb{E}_0 \left[e^{k \int_0^T A(X(t)) dt} \right]$, the average is taken over the model statistics \mathbb{P}_0 . In large deviation theory (see e.g. (36)), $\lambda(k) = \lim_{T \rightarrow \infty} \lambda(k, T)$ with $\lambda(k, T) = \frac{1}{T} \log Z(k, T)$ is called a scaled cumulant generating function. One can prove that for large times, the PDF $P(a, T)$ of time averaged temperature a , satisfies $P(a, T) \underset{T \rightarrow \infty}{\asymp} e^{-T I[a]}$. Whenever I is convex, λ and I are the Legendre–Fenchel transform of one another: $\lambda(k) = \sup_a \{ka - I(a)\}$ and $I(a) = \sup_k \{ka - \lambda(k)\}$. The reader knowledgeable of statistical mechanics or thermodynamics will immediately notice the analogies between Z and the partition function, a and the energy, k and the temperature, λ and the free energy, and between I and the entropy. To summarize, the large deviation algorithm allows us to choose the “temperature” k for which dynamical states of “energy” a (in this case time averaged European temperature) will become common. Increasing k we can thus study events with more and more extreme heat waves.

Return times for 90 day heat waves

We use the large deviation algorithm and formula (2) in order to compute the return times for heat waves lasting several weeks, following the methodology described in the Supporting Information Appendix. Fig. 4 shows return times versus amplitude $a = \frac{1}{T} \int_0^T \tilde{A}(t) dt$, for $T = 90$ days. The black curve has been plotted from a 1000 year control run. The

red curve has been obtained as explained in the Supporting Information Appendix from six experiments with the large deviation algorithm with values of the bias parameter k ranging from 10 to 40 (see Eq. (2)). Each of these simulations has a computational cost of about 182 years.

The first striking result on Fig. 4 is that we can compute return times up to $10^6 - 10^7$ years with a total computational cost of the order of 10^3 years. This is thus a gain of more than three orders of magnitude in the sampling efficiency. It is striking that we can compute the return times for events that could not have been observed in a direct numerical simulation with the current or foreseeable computational possibilities.

Another aspect is the improvement of the quality of the statistics. In the control run there is only one heat wave with temperature in excess of 2K during 90 days, while in the $k = 50$ experiment there are several hundreds, at a fraction of the computational cost. We can thus recover the return time of such heat waves at either a much smaller numerical cost compared with the control run, or with a much smaller relative error, for a given numerical cost. Such an improvement of the statistics will be crucial to perform a dynamical analysis that involves temperature and pressure fields, as discussed below.

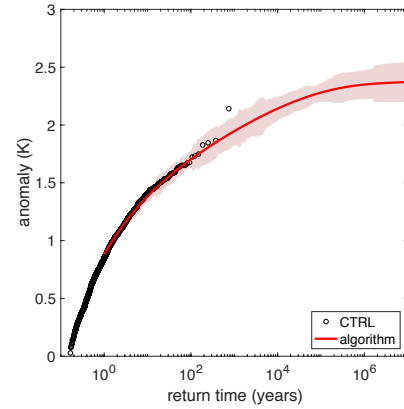


Fig. 4. Return times for the 90 day Europe surface temperature, computed from the 1000 years long control run (black) and from the the large deviation algorithm, at the same computational cost as the control run (red). This illustrates both the good overlap on the (10, 300) year range, and the fact that the algorithm can predict probability for events that can not be observed in the control run.

Teleconnection patterns for extreme heat waves

We use the excellent statistics gathered with the large deviation algorithm in order to describe the corresponding state of the atmosphere during extreme heat waves events. Fig. 5(a) shows the temperature and the 500hPa geopotential height anomalies, conditioned on the occurrence of a 90 day 2°K heat wave (composite statistics). Those conditional statistics are reminiscent of the teleconnection pattern maps sometimes shown in the climate community. However while usual teleconnection patterns are computed from empirical orthogonal function (EOF) analysis, and thus describe typical fluctuations, our extreme event conditional statistics describe very rare flows that characterize extreme heat waves. Those global maps are a new way to consider rare event and the atmosphere fluctuation statistics, which is extremely interesting from a dynamical point of view.

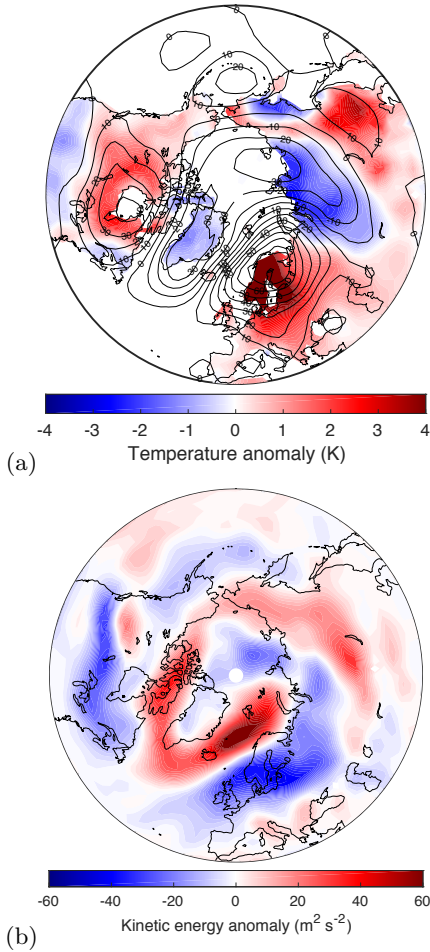


Fig. 5. (a) Northern hemisphere surface temperature anomaly (colors), and 500 hPa geopotential height anomaly (contours), conditional on the occurrence of heat wave conditions $\frac{1}{T} \int_0^T A(x_n(t))dt > a$, with $T = 90$ days and $a = 2$ K, estimated from large deviation algorithm. (b) Northern hemisphere anomaly of the averaged kinetic energy for the zonal velocity at 500 hPa conditional on the occurrence of heat wave conditions $\mathbb{E} [K E_{500} | \frac{1}{T} \int_0^T A(x_n(t))dt > a]$, with $T = 90$ days and $a = 2$ K, estimated from the large deviation algorithm, with respect to the long time average $\mathbb{E} [K E_{500}]$ computed from the control run.

By definition, as we plot statistics conditioned on $a = \frac{1}{T} \int_0^T A(x_n(t))dt > 2^\circ\text{K}$, with $T = 90$ days, Fig. 5(a) shows a warming pattern over Europe. The geopotential height map also shows a strong anticyclonic anomaly right above the area experiencing the maximum warming, as expected through the known positive correlation between surface temperature and anticyclonic conditions (34). A less expected and striking result is that the strong warming over Europe is correlated with a warming over South Eastern Asia, and a warming over North America, both with substantial surface temperature anomalies of order of 1 K to 3 K, and anti-correlated with strong cooling over Russia and Greenland, of the order of -1 K to -2 K. This teleconnection pattern is due to a strongly non linear stationary pattern for the jet stream, with a wavenumber 3 dominating the pattern, as is clearly seen from the geopotential height anomaly. On Fig. 5(b), the anomaly of the kinetic energy, gives a complementary view: over Europe, the succession of a southern blue band (negative anomaly), and a northern red band (positive anomaly) should be interpreted as a northward

shift of the jet stream there. Strikingly, over Greenland and North America, the jet stream is at the same position (but it is more intense) for the large deviation algorithm statistics as for the control run, while it is shifted northward over Europe and very slightly southward over Asia. This is related to the strong southwest-northeast tilt of the geopotential height anomalies over the Northern Atlantic. The extended red area (positive anomaly of kinetic energy) over Asia is rather due to a more intense cyclonic activity there, than to a change of jet stream position.

Inspection of the time series of the daily temperature shows that along the long duration of heat waves, the synoptic fluctuations on times scales of weeks are still present (see also Figure 2b)). The temperature is thus fluctuating with fluctuations of order of 5 to 10 degrees, as usual, but they fluctuate around a larger temperature value than usual. This is also consistent with the northward shift of the jet stream over Europe, but does not seem to be consistent with a blocking phenomenology as hypothesized in many other publications. This calls for using similar large deviation algorithms with other models and other setups to test the robustness of the present observation.

Conclusions

We have demonstrated that rare event algorithms, developed using statistical physics ideas, can improve the computation of the return times and the dynamical aspects of extreme heat waves. One of the future challenge in the use of rare event algorithms for studying climate extreme will be to identify which algorithms and which score functions will be suitable for each type of rare event. We anticipate that this new tool will open a range of completely new studies that were out of scope so far. First it will pave the way to the use of state of art climate model to study rare extreme events, without having to run the model for unaffordable times. The demonstrated gain of several orders of magnitude in the sampling efficiency will also help to make quantitative model comparison, in order to assess on a more quantitative basis the skill to predict extreme events, for the existing models. It will also open a new range of dynamical studies. As an example, having an high number of heat waves allowed us to conclude that a Europe heat wave, mainly affecting Scandinavia, is rather related to a Northward jet-stream shift rather than a Rossby wave breaking, in the Plasim model. Such a phenomenology may well be model and model resolution dependent. Finally, and may be more importantly, this new tool will be extremely useful in the near future to assess quantitatively anthropogenic carbon dioxide emission impact on heat waves and other classes of extreme events. Assessment of the anthropogenic causes of rare event return time changes requires to compare two different climates (4, 33), and to run a rare event algorithm for each case.

SI Appendix

The Supporting Information Appendix contains a complete description of the GKL algorithm, of the method to compute return times with rare event algorithm, the description of the implementation of the Plasim model, aspects of the statistical post processing, and the description of the dynamical quantities represented in this article.

ACKNOWLEDGMENTS. The authors would like to thank

Gualtiero Badin, Edilbert Kirk, and Thibault Lestang for useful discussions and suggestions on various aspects of this work. JW and FR acknowledge the support of the AXA Research Fund.

1. IPCC (2012) *Managing the risks of extreme events and disasters to advance climate change adaptation: special report of the Intergovernmental Panel on Climate Change*. (Cambridge University Press, New York, NY).
2. AghaKouchak A (2012) *Extremes in a changing climate detection, analysis and uncertainty*. (Springer, Dordrecht; New York).
3. Herring SC, Hoerling MP, Peterson TC, Stott PA (2014) Explaining Extreme Events of 2013 from a Climate Perspective (http://www2.ametsoc.org/ams/assets/File/publications/BAMS_EEE_2013_Full_Report.pdf).
4. IPCC (2013) *Climate Change 2013: The Physical Science Basis. Contribution of Working Group I to the Fifth Assessment Report of the Intergovernmental Panel on Climate Change*. (Cambridge University Press, Cambridge, United Kingdom and New York, NY, USA).
5. Coumou D, Rahmstorf S (2012) A decade of weather extremes. *Nature Climate Change* 2(7):491–496.
6. Shepherd T (2015) Dynamics of temperature extremes. *Nature* 522:425–427.
7. Shepherd TG (2016) A common framework for approaches to extreme event attribution. *Current Climate Change Reports* 2(1):28–38.
8. Robine JM, et al. (2008) Death toll exceeded 70,000 in Europe during the summer of 2003. *Comptes Rendus Biologies* 331(2):171–178.
9. Barriopedro D, Fischer EM, Luterbacher J, Trigo RM, Garcia-Herrera R (2011) The Hot Summer of 2010: Redrawing the Temperature Record Map of Europe. *Science* 332(6026):220–224.
10. E W, Ren W, Vanden-Eijnden E (2003) Energy landscape and thermally activated switching of submicron-sized ferromagnetic elements. *Journal of Applied Physics* 93(4):2275–2282.
11. Kohn RV, Reznikoff MG, Vanden-Eijnden E (2005) Magnetic Elements at Finite Temperature and Large Deviation Theory. *Journal of Nonlinear Science* 15(4):223–253.
12. Rolland J, Bouchet F, Simonnet E (2016) Computing transition rates for the 1-d stochastic Ginzburg-Landau-Allen-Cahn equation for finite-amplitude noise with a rare event algorithm. *Journal of Statistical Physics* 162(2):277–311.
13. Chandler D (2005) Interfaces and the driving force of hydrophobic assembly. *Nature* 437(7059):640–647.
14. Noé F, Schütte C, Vanden-Eijnden E, Reich L, Weikl TR (2009) Constructing the equilibrium ensemble of folding pathways from short off-equilibrium simulations. *Proceedings of the National Academy of Sciences* 106(45):19011–19016.
15. Metzner P, Schütte C, Vanden-Eijnden E (2006) Illustration of transition path theory on a collection of simple examples. *The Journal of Chemical Physics* 125(8):084110.
16. Bolhuis PG, Chandler D, Dellago C, Geissler PL (2002) Transition Path Sampling: Throwing Ropes Over Rough Mountain Passes, in the Dark. *Annual Review of Physical Chemistry* 53(1):291–318.
17. Wolde PRT, Frenkel D (1997) Enhancement of Protein Crystal Nucleation by Critical Density Fluctuations. *Science* 277(5334):1975–1978.
18. Laurie J, Bouchet F (2015) Computation of rare transitions in the barotropic quasi-geostrophic equations. *New Journal of Physics* 17(1):015009.
19. Grafke T, Grauer R, Schäfer T (2013) Instanton filtering for the stochastic burgers equation. *Journal of Physics A: Mathematical and Theoretical* 46(6):062002.
20. Grafke T, Grauer R, Schäfer T, Vanden-Eijnden E (2014) Arclength parametrized hamilton's equations for the calculation of instantons. *Multiscale Modeling & Simulation* 12(2):566–580.
21. Bouchet F, Laurie J, Zaboronski O (2014) Langevin dynamics, large deviations and instantons for the quasi-geostrophic model and two-dimensional euler equations. *Journal of Statistical Physics* 156(6):1066–1092.
22. Bouchet F, Marston J, Tangarife T (2017) Fluctuations and large deviations of Reynolds' stresses in zonal jet dynamics. *arXiv preprint arXiv:1706.08810*.
23. Kahn H, Harris TE (1951) Estimation of particle transmission by random sampling. *National Bureau of Standards applied mathematics series* 12:27–30.
24. Rubino G, Tuffin B (2009) *Rare event simulation using Monte Carlo methods*. (Wiley, Chichester, U.K).
25. Bucklew JA (2004) *An introduction to rare event simulation*. (Springer, New York).
26. Del Moral P (2004) *Feynman-Kac Formulae Genealogical and Interacting Particle Systems with Applications*. (Springer New York, New York, NY).
27. Bréhier CE, Lelièvre T, Rousset M (2014) Analysis of Adaptive Multilevel Splitting algorithms in an idealized case. *arXiv:1405.1352 [math]*. arXiv: 1405.1352.
28. Cérou F, Guyader A (2007) Adaptive Multilevel Splitting for Rare Event Analysis. *Stochastic Analysis and Applications* 25(2):417–443.
29. Giardinà C, Kurchan J, Peliti L (2006) Direct Evaluation of Large-Deviation Functions. *Physical Review Letters* 96(12):120603.
30. Tailleur J, Kurchan J (2007) Probing rare physical trajectories with Lyapunov weighted dynamics. *Nature Physics* 3(3):203–207. WOS:000244558400021.
31. Lecomte V, Tailleur J (2007) A numerical approach to large deviations in continuous time. *Journal of Statistical Mechanics: Theory and Experiment* 2007(03):P03004.
32. Fraedrich K, Jansen H, Luksch U, Lunkeit F (2005) The Planet Simulator: towards a user friendly model. *Meteorol. Z.* 14:299–304.
33. Otto F, Massey N, van Oldenborgh G, Jones R, Allen M (2012) Reconciling two approaches to attribution of the 2010 russian heat wave. *Geophys. Res. Lett.* 39:L04702.
34. Stefanon M, D'Andrea F, Drobninski P (2012) Heatwave classification over Europe and the Mediterranean region. *Environmental Research Letters* 7:014023.
35. Fischer EM, Schär C (2010) Consistent geographical patterns of changes in high-impact European heatwaves. *Nature Geoscience* 3(6):398–403.
36. Touchette H (2009) The large deviation approach to statistical mechanics. *Physics Reports* 478:1–69.
37. Giardinà C, Kurchan J, Lecomte V, Tailleur J (2011) Simulating Rare Events in Dynamical Processes. *Journal of Statistical Physics* 145(4):787–811.
38. Wouters J, Bouchet F (2016) Rare event computation in deterministic chaotic systems using genealogical particle analysis. *J. Phys. A: Math. Theor.* 49:374002.
39. Ruelle D (1998) General linear response formula in statistical mechanics, and the fluctuation-dissipation theorem far from equilibrium. *Physics Letters A* 245(3-4):855–870.
40. Ruelle D (2009) A review of linear response theory for general differentiable dynamical systems. *Nonlinearity* 22(4):855–870.
41. Gallavotti G (1996) Chaotic hypothesis: Onsager reciprocity and fluctuation-dissipation theorem. *Journal of Statistical Physics* 84:899–926.
42. Rohwer CM, Angeletti F, Touchette H (2015) Convergence of large-deviation estimators. *Phys. Rev. E* 92(5):052104.
43. Hoskins BJ, James IN (2014) *Fluid Dynamics of the Midlatitude Atmosphere*. (John Wiley & Sons, Ltd).

Supporting Information (SI) appendix

SI Data and Methods

Giardina–Kurchan–Tailleur–Lecomte algorithm. Rare event algorithms have first been proposed and developed in the 50's (23), and they have since then been used for a wide range of applications. A partial mathematical analysis of these algorithms is now available (26).

The general idea is the following. We let evolve in parallel an ensemble of trajectories of a numerical model starting from different initial conditions. After a given *resampling time* some members of the ensemble are killed and some others are cloned, depending on the values of weights defined on the past evolution of the trajectories. In this way the trajectory probability measure is tilted with respect to the “natural” model trajectory probability measure. How the distribution will be tilted will depend on the definition of the weights, which can be defined in order to target the extremes of an observable of interest.

In the algorithm used in this work, the weights are chosen such that the measure is tilted in order to favor trajectories characterized by large values of a chosen time averaged observable. This form of a rare event algorithm has first been proposed by (29) and has been used for instance to study finite time Lyapunov exponents (30). As the primary aim of this algorithm is to compute large time large deviation rate function, we call this algorithm the *Giardina–Kurchan–Lecomte–Tailleur large deviation algorithm*, or simply the

large deviation algorithm.

We perform simulations of an ensemble of N trajectories $\{X_n(t)\}$ (with $n = 1, 2, \dots, N$) starting from different initial conditions. The total integration time of the trajectories is denoted T_a . In the limit of large T_a , the initial conditions affect only a transient regime. We consider an observable of interest $A(X(t))$ (in this study the Europe temperature) and a resampling time τ . At times $t_i = i\tau$ (with $i = 1, 2, \dots, T_a/\tau$) we assign to each trajectory n a weight W_n^i defined as

$$W_n^i = \frac{e^{k \int_{t_{i-1}}^{t_i} A(X_n(t)) dt}}{R_i} \quad \text{with} \quad R_i = \frac{1}{N} \sum_{n=1}^N e^{k \int_{t_{i-1}}^{t_i} A(X_n(t)) dt}. \quad [3]$$

For each trajectory X_n , a random number of copies of the trajectory are generated, on average proportional to the weight W_n^i and such that the total number of trajectories produced at each event is equal to N . The parameter k is chosen by the user in order to control the strength of the selection and thus to target a class of extreme events of interest. The larger the value of k , the more trajectories with large values of the time average observable will survive the selection.

Let us denote $\mathbb{P}_0(\{X(t)\}_{0 \leq t \leq T_a})$ the probability to observe a trajectory $\{X(t)\}_{0 \leq t \leq T_a}$ in the model, and $\mathbb{P}_k(\{X(t)\}_{0 \leq t \leq T_a})$ the probability to observe the same trajectory with the algorithm. By construction of the algorithm through the weights (3) we have that

$$\mathbb{P}_k(\{X(t)\}_{0 \leq t \leq T_a} = \{x(t)\}_{0 \leq t \leq T_a}) \underset{N \rightarrow \infty}{\sim} \frac{e^{k \int_0^{T_a} A(x(t)) dt}}{\mathbb{E}_0 \left[e^{k \int_0^{T_a} A(x(t)) dt} \right]} \mathbb{P}_0(\{X(t)\}_{0 \leq t \leq T_a} = \{x(t)\}_{0 \leq t \leq T_a}). \quad [4]$$

where \mathbb{E}_0 mean an average over \mathbb{P}_0 , and $\underset{N \rightarrow \infty}{\sim}$ means that this is true only asymptotically for large N with typical error of order $1/\sqrt{N}$ when evaluating averages over observables. Equation (4) is obtained by assuming the mean field approximation

$$R_1 = \frac{1}{N} \sum_{n=1}^N e^{k \int_0^{\tau} A(X_n(t)) dt} \underset{N \rightarrow \infty}{\sim} \mathbb{E}_0 \left[e^{k \int_0^{\tau} A(X_n(t)) dt} \right], \quad [5]$$

which, by induction, and using a formula similar to (5) at each step of the induction, leads to

$$\prod_{i=1}^{T_a/\tau} R_i \underset{N \rightarrow \infty}{\sim} \mathbb{E}_0 \left[e^{k \int_0^{T_a} A(X_n(t)) dt} \right] \quad [6]$$

(see (29, 37)).

The validity of the mean field approximation and the fact that the typical relative error due to this approximation is of order $1/\sqrt{N}$ has been proven to be true for a family of rare event algorithms including the one adopted in this paper by (26).

Formula (4) is valid only for times T_a that are integer multiples of the resampling time τ . The killed trajectories have to be discarded from the statistics. Starting from the final N trajectories at time T_a , one goes backwards in time through the selection events attaching to each piece of trajectory its ancestor. In this way one obtains an effective ensemble of N trajectories from time 0 to time T_a , distributed according to \mathbb{P}_k . All trajectories reconstructed in this way are real solutions of the model, so that we are not changing the dynamics, but only sampling trajectories according to the distribution \mathbb{P}_k rather than according to the distribution \mathbb{P}_0 .

In the normalization term $Z(k, T) = \mathbb{E}_0 \left[e^{k \int_0^T A(X(t)) dt} \right]$, the average is taken over the model statistics \mathbb{P}_0 . In large deviation theory (see e.g. (36)), $\lambda(k) = \lim_{T \rightarrow \infty} \lambda(k, T)$ with $\lambda(k, T) = \frac{1}{T} \log Z(k, T)$ is called a scaled cumulant generating function. One can prove that for large times, the PDF $P(a, T)$ of time averaged temperature a , satisfies $P(a, T) \underset{T \rightarrow \infty}{\sim} e^{-T I[a]}$. Whenever I is convex, λ and I are the Legendre–Fenchel transform of one another: $\lambda(k) = \sup_a \{ka - I(a)\}$ and $I(a) = \sup_k \{ka - \lambda(k)\}$. The reader knowledgeable of statistical mechanics or thermodynamics will immediately notice the analogies between Z and the partition function, a and the energy, k and the temperature, λ and the free energy, and between I and the entropy. To summarize, the large deviation algorithm allows us to choose the “temperature” k for which dynamical states of “energy” a (in this case time averaged European temperature) will become common.

By construction (29, 37) the algorithm gives an estimator of the scaled cumulant generating function of $A(X(t))$

$$\lambda(k) = \lim_{T \rightarrow \infty} \lambda(k, T) \quad \text{with} \quad \lambda(k, T_a) = \frac{1}{T_a} \sum_{i=1}^{T_a/\tau} \log R_i, \quad [7]$$

with a relative error of order $1/\sqrt{N}$.

While the GKLT algorithm has been initially designed to compute large deviation rate function, we can use it to compute any statistical quantity related to the statistic \mathbb{P}_0 , from the \mathbb{P}_k . This is done using the backward reconstructed trajectories and inverting formula (4). If one for example want to estimate the expectation value of an observable $O(\{X(t)\}_{0 \leq t \leq T_a})$ of the model, an estimator is thus

$$\mathbb{E}_0 \left[O \left(\{X(t)\}_{0 \leq t \leq T_a} \right) \right] \underset{N \rightarrow \infty}{\sim} \frac{1}{N} \sum_{n=1}^N O \left(\{X_n(t)\}_{0 \leq t \leq T_a} \right) e^{-k \int_0^{T_a} A(X_n(t)) dt} e^{\tau_a \lambda(k, T_a)}, \quad [8]$$

where the X_n are the N backward reconstructed trajectories. Empirical estimators of quantities related to rare (for \mathbb{P}_0) events of the kind of 8 (thus using data distributed according to \mathbb{P}_k) have a dramatically lower statistical error, due to the larger number of relevant rare events present in the effective ensemble.

Algorithm implementation. We describe the large deviation algorithm implementation. Start with N trajectories, each with different initial conditions, for instance sampled through an ensemble of statically independent states obtained from a control run. For $i = 1, \dots, T_a/\tau$

1. Iterate each trajectory from time $t_{i-1} = (i-1)\tau$ to time $t_i = i\tau$;
2. At time t_i stop the simulation and assign to each trajectory n a weight

$$W_n^i = \frac{e^{k \int_{t_{i-1}}^{t_i} A(X_n(t)) dt}}{R_i} \quad [9]$$

with

$$R_i = \frac{1}{N} \sum_{n=1}^N e^{k \int_{t_{i-1}}^{t_i} A(X_n(t)) dt}. \quad [10]$$

3. Compute the number of copies produced by each trajectory as

$$c_n^i = \lfloor W_n^i + u_n \rfloor \quad [11]$$

where $\lfloor \cdot \rfloor$ is the integer part and the u_n are N independent random numbers uniformly distributed between 0 and 1. When $c_n^i = 0$ the corresponding trajectory is killed;

4. The number of trajectories present after the selection operation is

$$N_i = \sum_{n=1}^N c_n^i \quad [12]$$

5. Compute then the difference $\Delta N_i = N_i - N$. If $\Delta N_i > 0$, then ΔN_i trajectories are randomly selected (without repetition) and killed. If $\Delta N_i < 0$, then $|\Delta N_i|$ trajectories are randomly selected (with repetition) and cloned.
6. Reinitialize the state of the N ensemble members at time t_i according to the cloning, and restart from point 1 incrementing i by 1.

The ΔN_i trajectories to be killed/cloned are chosen among the N_i trajectories present after the killing/cloning event, not among the N trajectories present before the killing/cloning event. In the case $\Delta N_i < 0$, only trajectories for which $c_n^i > 0$ are allowed to be cloned. Operations 3-5 guarantee that the number of ensemble members remains constant throughout the evolution of the system (37). After an initial transient the algorithm ensemble reach a statistically stationary state, and the memory of the initial conditions is lost.

The N initial conditions should be independent and provide a reasonable sampling of the attractor of the system. A possible way to create the initial conditions is to generate a control run of the model, and take states of the system separated by long enough times so that they are statistically independent. In our study we have created a 1000 year control run (also used as a benchmark for the performances of the algorithm). From this, we have taken 1000 model states, at one year intervals, as our set of initial conditions. If we would have not needed a control run, we could have used initial conditions taken every week (which is about the correlation time of the dynamics for this model). It is essential to note that the duration of the run to prepare independent initial conditions is smaller by several orders of magnitudes than the return times that can be computed using the algorithm.

Tests performed with the Ornstein-Uhlenbeck process and the Lorenz 63 model suggest that the resampling time τ should be

not larger than the Lyapunov time of the model, and sufficiently larger than the numerical time step. Between these two limits the performances of the algorithm seems to be insensitive to the specific choice of τ . Here we have taken $\tau = 8$ days, close to the autocorrelation time of the European surface temperature in Plasim, that is $\tau_c \approx 7.5$ days.

Dealing with a deterministic system, two clones of the same trajectory will evolve exactly in the same way. In order to have copies of the same trajectory that actually separate in the following time evolution, we add a small random perturbation to the state of the trajectories at time t_i , immediately after the reinitialization according to the cloning (38). The perturbation is introduced adding to the coefficients of the spherical harmonics of the logarithm of the surface pressure a set of random numbers, sampled independently according to a uniform distribution in $[-\epsilon\sqrt{2}, \epsilon\sqrt{2}]$, with $\epsilon = 10^{-4}$. On average the relative perturbation (computed as the difference between the root mean square of the spherical harmonic coefficients before and after the perturbation, divided by the root mean square of the spherical harmonic coefficients) is of order $\sim 7.5 \cdot 10^{-5}$. Assuming linear response to external perturbations for the statistics of the system (the invariant measure of the system) (39, 40), under the the Chaotic Hypothesis (41) (exploiting the chaoticity of the dynamics and the large number of degrees of freedom), the statistical properties of the system are thus expected to be altered by an error of order of the perturbation. This is way lower than any other errors, for instance sampling errors.

Plasim model and setup. The numerical model used in this study is the Planet Simulator (Plasim) (32). Plasim is a spectral intermediate complexity general circulation model with a full set of physical parameterizations for unresolved processes. It produces a fairly realistic present climate and is representative of the class of complex numerical models used for climate prediction, although it is computationally less demanding than contemporary IPCC-standard climate models. See the Reference Manual at <https://github.com/Edilbert/PLASIM> for a detailed description.

We set the model at T42 horizontal resolution and 10 levels vertical resolution, for a total of $O(10^5)$ degrees of freedom. The time step is 30 minutes and output is stored every 6 hours. The model runs in perpetual summer conditions, with no daily nor seasonal cycle. The boundary conditions (sea surface temperature, ice coverage, and radiative forcing at top of the atmosphere) are set to climatological values for July 16th. The choice of a perpetual summer simulation is for convenience: running the large deviation algorithm is simpler in this context. We will add a seasonal cycle in a forthcoming work. We consider as test observable the surface temperature in the atmospheric layer 2m above the ground, averaged over the land area with latitudinal and longitudinal boundaries 36N-70N, 11W-25E respectively (so called Europe surface temperature in the main text).

A 1000 year long control run (CTRL_LONG) is taken as a benchmark for the statistics. A shorter run (CTRL_SHORT) consisting of the last 284 years of the CTRL_LONG run is used to compare the performances of the algorithm against direct sampling.

The experiment with the large deviation algorithm with $k = 2$ is performed with $N = 128$ trajectories. The integration time of each trajectory is $T_a = 800$ days, thus the computational cost is $C = NT_a \approx 284.4$ years. The resampling time is set at $\tau = 8$ days, which is of the order of the autocorrelation time $\tau_c = 7.5$ days of the Europe averaged temperature.

Figure S6 shows how the scaled cumulant generating function λ estimated from the large deviation algorithm with $k = 2$ at a numerical cost of 248 years, is at least as good as the one estimated from a control run lasting 1000 years, and is much better than the one estimated from a control run lasting 248 years. This is a consistency test between the large deviation algorithm and the direct use of the model, which confirms the robustness of the procedure we have followed (including the perturbation of the trajectories).

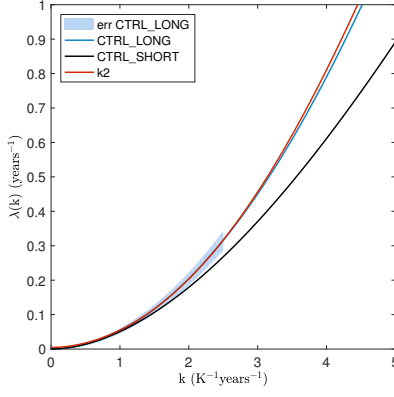


Fig. S6. The scaled cumulant generating function $\lambda(k)$ estimated from the large deviation algorithm with $k = 2$ at a numerical cost of 248 years (red line), is at least as good as the one estimated from a control run lasting 1000 years (blue line), and is much better than the one estimated from a control run lasting 248 years (black line). The shaded area corresponds to 1 standard deviation related to the empirical average.

We have then performed six experiments with much larger values of k , in order to compute efficiently the statistics of extreme heat waves. We have taken $k = 10, 20, 40$ and 50 . The experiments with $k = 20$ and 40 have been performed twice with different initial conditions. We have taken $N = 512$ trajectories, each 128 days long, and the resampling time is again set to 8 days.

In order to demonstrate that the algorithm actually reduces the variance, we have computed the relative error on the estimate of surface temperature and of the 500 hPa geopotential height, comparing a control run and the statistics of the large deviation algorithm. The results (not presented) show that the empirical variance is way lower using the large deviation algorithm, than using the control run.

Plotting return time curves using the large deviation algorithm.

Return time plots for rare events sampled from a timeseries. Let us consider a stochastic process $\{Y(t)\}$ and a threshold value a . We define the random variable $\tau(a, t) = \min\{\tau \geq t | Y(\tau) > a\}$. Then the return time with threshold a is defined as

$$r(a) = \mathbb{E}(\tau(a, t)), \quad [13]$$

where \mathbb{E} is the average over the realization of the process. Let us consider the estimate of $r(a)$ from a sample timeseries of duration T_d : $\{Y(t)\}_{0 \leq t \leq T_d}$. Let us consider a rare value a such that most of the times $Y(t) < a$, or equivalently $r(a) \gg \tau_c$ where τ_c is the correlation time of the process. The return time $r(a)$ is then the average time one has to wait in between two statistically independent events exceeding the value a .

Let us divide the timeseries $\{Y(t)\}_{0 \leq t \leq +\infty}$ in pieces of duration $\Delta T \gg \tau_c$, and let us define $a_m = \max\{Y(t) | (m-1)\Delta T \leq t \leq m\Delta T\}$ and $s_m(a) = 1$ if $a_m > a$ and 0 otherwise. With generic hypothesis on the loss of memory for the process, the number of events $N(t) = \sum_m s_{\lfloor t/\Delta T \rfloor}$ is then well approximated by a Poisson process with density $\lambda(a) = 1/r(a)$, asymptotically when $r(a) \gg \tau_c$. An estimate of $r(a)$ is then

$$r(a) = -\frac{\Delta T}{\log\left(1 - \frac{1}{M} \sum_{m=1}^M s_m(a)\right)}. \quad [14]$$

We then rank the sequence $\{a_m\}_{1 \leq m \leq M}$ in decreasing order and denote the ranked sequence $\{\tilde{a}_m\}_{1 \leq m \leq M}$ such that $\tilde{a}_1 \geq \tilde{a}_2 \geq \dots \geq \tilde{a}_M$. Using the estimate (14) we associate to the threshold \tilde{a}_m the return time $r(\tilde{a}_m) = -\frac{\Delta T}{\log\left(1 - \frac{m}{M}\right)}$. The return time plot is then the plot $r(\tilde{a}_m)$ as a function of \tilde{a}_m , as illustrated for instance on figure S7.

Return time plots sampled using the large deviation algorithm. The large deviation algorithm provides an effective ensemble of trajectories. For each of these trajectories, we compute $A_n(T, t) = \frac{1}{T} \int_t^{T+t} A(X_n(t)) dt$ and compute maxima over the trajectory $a_n = \max_{0 \leq t \leq T_a - T} \{A_n(T, t)\}$. Rather than providing just a sequence $\{a_n\}_{1 \leq n \leq N}$, the large deviation algorithm provides a sequence $\{a_n, p_n\}_{1 \leq n \leq N}$ where each trajectory, and thus each maxima a_n , is associated with a probability p_n of observing this value in the model. The probability p_n is computed from equation (8): $p_n = \frac{1}{N} e^{-k \int_0^{T_a} A(X_n(t)) dt} e^{T_a \lambda(k, T_a)}$. As a consequence, the generalization of formula (14) is straightforward and leads to

$$r(a) = -\frac{T_a - T}{\log\left(1 - \sum_{n=1}^N p_n s_n(a)\right)}, \quad [15]$$

(we recall that $s_n(a) = 1$ if $a_n > a$ and 0 otherwise, $\Delta T = T_a - T$ is the length of the considered timeseries for each $A_n(T, t)$). In practice, to plot the return time curve, we rank the sequence $\{a_n, p_n\}_{1 \leq n \leq M}$, sort it in decreasing order for the values of a , and denote the ranked sequence $\{\tilde{a}_n, \tilde{p}_n\}_{1 \leq n \leq M}$ such that $\tilde{a}_1 \geq \tilde{a}_2 \geq \dots \geq \tilde{a}_N$. We then associate to the threshold \tilde{a}_m the return time

$$r(\tilde{a}_m) = -\frac{T_a - T}{\log\left(1 - \sum_{m=1}^N \tilde{p}_m\right)}, \quad [16]$$

as the average number of events that have been observed with an amplitude larger than \tilde{a}_m is $\sum_{m=1}^N \tilde{p}_m$. The return time plot is then the plot $r(a)$ as a function of a , as illustrated for instance on figure S7.

As a benchmark, the following section illustrates that return time plots sampled from the algorithm coincide the return time sampled from the timeseries of the Ornstein–Uhlenbeck process and can be computed at a much smaller computation cost.

Test of the algorithm for the Ornstein–Uhlenbeck process. Figure S7 shows the algorithm benchmark for the Ornstein–Uhlenbeck process: the dynamics $dx = -xdt + dW_t$ where W_t is the Wiener process ($\frac{dW_t}{dt}$ is a Gaussian noise with correlations $\mathbb{E}\left(\frac{dW_t}{dt} \frac{dW_{t'}}{dt'}\right) = \delta(t - t')$). We study rare events for the time average observable $A(t) = \frac{1}{T} \int_t^{T+t} x(t) dt$ with $T = 50$. $r(a)$ is the return time for this observable with amplitude a (please see definition (13)). We first sample $r(a)$, using formula (14), from a single realization of the Ornstein–Uhlenbeck process, of total duration $T_d = 10^9$ (control run). The result is shown as a black dashed line on both figures S7a) and b). The blue plain curve on figure S7a) has been sampled using the large deviation algorithm, with a duration per trajectory $T_a = 100$, a clone number $N = 600$, and a cloning time $\tau = 0.5$. The algorithm has been run $K = 100$ times to gather statistics. The total numerical cost is thus $T_{tot} = T_a * N * K = 6.10^6$, which is 160 times less than the total duration T_d for the control run. The parameter k has been set to $k = 0.3$ such that events with a threshold $0.6 < a < 0.7$ are typical. The result shows a perfect comparison with the control run up to return times of order 5.10^7 (much longer than the total numerical cost) and an agreement with error of order 10% for return times $5.10^7 < r(a) < 5.10^8$. This shows that the algorithm computes extremely well the return time plot at a much lower numerical cost. Figure S7a) show the same results, but using only 10 algorithm realizations for a total cost 1600 times less than the total duration T_d for the control run.

Statistical postprocessing. All the statistical postprocessing has been performed in Matlab environment. In particular, the probability distribution functions in Fig. 3(b) have been computed using a kernel density estimation method.

The direct estimate of the scaled cumulant generating function from the control run has been obtained following (42). In particular, the error bar in Fig. 4(a) is computed taking one standard deviation of the empirical sum of the estimator proposed in (42), limited to the region of Gaussian convergence.

The estimate of the return time curve in general has been obtained as explained in Section 4. In particular, the estimate from the algorithm (red line of Fig 4(b)) has been obtained by joining

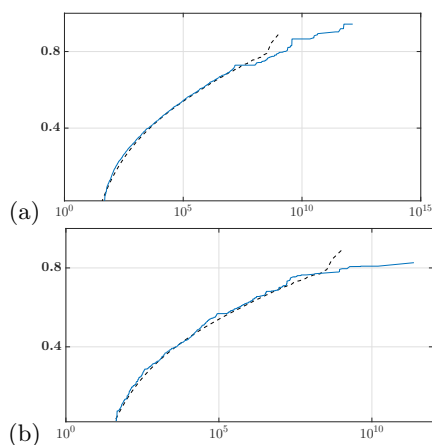


Fig. S7. Amplitude versus return times for the Ornstein-Uhlenbeck process, from a long control run (black dashed line) and the large deviation algorithm (blue curve). On panel a) 100 algorithm realizations have been used for a total cost 160 smaller than for the control run. On panel b) 10 algorithm realizations have been used for a total cost 1600 smaller than for the control run.

the results of six experiments, as follows. First we have computed for each experiment the return time curve $r(a)$ using formula (16), which gives plots $a(r)$. We have linearly interpolated the plots $a(r)$ on an equally spaced return time vector R ranging from 0 to 10^8 years. We have removed from each interpolated return time curve the anomalies that are outside one standard deviation around the mean, as we want to keep only the estimates that we consider reliable. We have then obtained a best estimate return time curve by averaging the tapered and interpolated return time curves from the individual experiments. Finally, the best estimate curve has been interpolated with a fifth order polynomial. The error bar is computed at each value of R as one standard deviation of the return time curves which have been averaged in order to obtain the best estimate at that value of R (usually 3 or 4 curves).

Featured dynamical quantities. The *geopotential* $\Phi(\phi, \lambda, z, t)$ is the gravitational potential energy per unit mass at latitude ϕ , longitude

λ , and elevation z

$$\Phi(\phi, \lambda, z) = \int_0^z g(\phi, \lambda, z') dz'$$

where g is the gravity acceleration. The *geopotential height* is the geopotential normalized to the standard gravity at mean sea level $g_0 = 9.80665 \text{ m s}^{-2}$

$$Z(\phi, \lambda, z) = \frac{\Phi(\phi, \lambda, z)}{g_0}$$

In atmospheric physics it is natural to define the vertical coordinate in terms of pressure p rather than in terms of geometric height z , assuming hydrostatic approximation (note that numerical climate models always assume hydrostatic balance in their set of equations). The geopotential height expressed in pressure coordinates behaves as a streamfunction for the geostrophic wind vector, that is the first order approximation of the wind vector for synoptic scale motions at the midlatitudes (see (43) for more details).

Contour plots of the anomalies of geopotential height in the mid-troposphere at 500 hPa (about 5500 m) can be used to visualize the state of the atmospheric circulation. Negative anomalies indicate low pressure systems (*cyclonic* anomalies, characterized by anticlockwise circulation in the Northern hemisphere and typically bad weather), while positive anomalies indicate high pressure systems (*anticyclonic* anomalies, characterized by clockwise circulation in the Northern hemisphere and typically fair weather). As discussed in the main text, heat waves are associated with persistent anticyclonic conditions, as shown in figure 5(a).

We call \mathbf{u}_{500} the velocity field vector at 500 hPa height. The zonal (West-East) component is u_{500} and the meridional (South-North) component is v_{500} . Let us define the contribution to the specific kinetic energy (the kinetic energy per unit mass) $KE_{500} = (u_{500}^2 + v_{500}^2)/2$. For example in figure 1b) in the text we show for the Northern hemisphere the long time average $\mathbb{E}[KE_{500}]$ from the control run. Large values of $\mathbb{E}[KE_{500}]$ correspond to areas of strong average zonal circulation in the mid-troposphere, hence to the average position of the storm track.